한국전산구조공학회
2002년도 가을 학술발표회 논문집

인발성형 적층 FRP 복합소재 재료상수의 해석적 추론

Analytical Prediction of Elastic Properties of Laminated Pultrusion FRP Composite Material

강 진 욱* Abdul Hamid Zureick**
Kang, Jin Ook

ABSTRACT

인발성형 적층 FRP 복합소재의 재료상수는 일반적으로 시편실험을 통해 구해지고 있으나, 본 논문에서는, 실험에서 구한 탄성계수가 부재일 경우를 위해, Micromechanics와 Classical Laminate Theory (CLT)를 이용한 적층 FRP 복합재료의 탄성계수(E_L과 E_L^b) 예측모델을 제시하였다. 또한 예측모델로부터 구한 값과 실험으로부터 얻은 실측값을 비교하여 그 적정성을 검증하였고, 예측모델의 민감도 및 확률적인 특성을 구성소재 (Constituents)의 재료특성에 근거해 평가하였다.

1. INTRODUCTION

The application of fiber-reinforced polymeric (FRP) composite structural shapes manufactured by the pultrusion process has grown very rapidly in the civil and structural engineering industry during the past 20 years. This is due to their excellent properties such as corrosion resistance, light weight, high strength to weight ratio, and high stiffness to weight ratio. The elastic properties of pultruded FRP composite components are mostly obtained from coupon tests or component tests. In the absence of experimental data, the elastic properties of laminated pultrusion FRP composite material may be analytically estimated based on micromechanics models and classical laminate theory (CLT).

This paper presents micromechanics models for the pultruded composite moduli, E_L and E_L^b. The moduli predicted based on the models were compared with those obtained experimentally. The characteristics of the models were assessed in a probabilistic approach based upon the inherent uncertainties of primitive variables, such as constituent material properties, fabrication process variables, and geometry of composites.

2. ANALYTICAL PREDICTION

2.1 Lamina Properties

The composite material used for this study consists of E-glass fibers, polyester resin, and fillers. The nominal elastic properties of the constituents are given in Table 1 which are based on Mallick's (1993), Katz & Mileswski's (1978), and manufacturer's data, where E is the Young's modulus, $G = E/2 \cdot (1+v)$ the shear modulus, $K = E/3 \cdot (1-2v)$ the bulk modulus, and v the Poisson's ratio.

* 정회원: 삼성물산(주) 건설부문 토목기술팀 차장 · 공학박사
** 조지아공대 (미국) 토목공학과 교수

Table 1: Nominal Elastic Properties of Composite Constituents

	E GPa (ksi)	G GPa (ksi)	K GPa (ksi)	v
E-glass fiber	72 (10,500)	30 (4,375)	40 (5,833)	0.2
Polyester resin	3.4 (490)	1.2 (179)	4.2 (609)	0.37
Kaolin clay filler	20 (2,900)	7.7 (1,115)	16.7 (2,417)	0.3

Based on the Reuss' method, the average shear modulus, G, and the average bulk modulus, K, of the matrix are computed as follows:

$$G = \frac{1}{\frac{v_{re}}{G_{re}} + \frac{v_{fil}}{G_{fil}}}$$
$$K = \frac{1}{\frac{v_{re}}{K_{re}} + \frac{v_{fil}}{K_{fil}}} \quad (1)$$

where v_{re} *and* v_{fil} are the volume ratios of the resin and fillers with respect to the matrix; e.g., v_{re}/v_m and v_{fil}/v_m, respectively. The Poisson's ratio, ν_m, the Young's modulus, E_m, and the shear modulus, G_m, of the matrix can be estimated by the following equations.

$$\nu_m = \frac{3K - 2G}{2G + 6K} \quad (2)$$

$$E_m = 2G(1 + \nu_m) \quad (3)$$

$$G_m = G \quad (4)$$

The evaluation results of the matrix elastic properties are given in Table 2.

Table 2: Matrix Elastic Properties

G GPa (ksi)	K GPa (ksi)	ν_m	E_m GPa (ksi)	G_m GPa (ksi)
1.45 (210)	4.85 (704)	0.36	3.95 (573)	1.45 (210)

The moduli of the roving layer reinforcements with respect to axes 1 and 2, shown in Figure 1, are estimated from Equation 5 (Chamis, 1984):

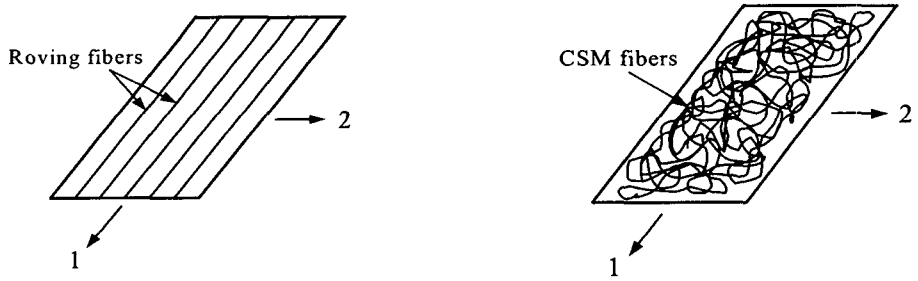

Figure 1: Reference Axes for Roving and CSM (Continuous Strand Mat) Layer Reinforcements

$$
\begin{aligned}
E_{11}^{rov} &= E_f \cdot v_{ef}^{rov} + E_m \cdot v_{em}^{rov} \\
E_{22}^{rov} &= \frac{E_m}{1-\sqrt{v_{ef}^{rov}} \cdot (1-\frac{E_m}{E_f})} \\
G_{12}^{rov} &= \frac{G_m}{1-\sqrt{e_{ef}^{rov}} \cdot (1-\frac{G_m}{G_f})} \\
\nu_{12}^{rov} &= v_{ef}^{rov} \cdot \nu_f + v_{em}^{rov} \cdot \nu_m \\
\nu_{21}^{rov} &= \frac{\nu_{12}^{rov} \cdot E_{22}^{rov}}{E_{11}^{rov}}
\end{aligned}
\tag{5}
$$

The moduli of the CSM layer reinforcements are evaluated using Equation 6 (Tsai and Pagano, 1968).

$$
\begin{aligned}
E^{csm} &= \frac{3}{8} \cdot E_{11}^{csm} + \frac{5}{8} \cdot E_{22}^{csm} \\
G^{csm} &= \frac{1}{8} \cdot E_{11}^{csm} + \frac{1}{4} \cdot E_{22}^{csm} \\
\nu^{csm} &= \frac{E^{csm}}{2 \cdot G^{csm}} - 1
\end{aligned}
\tag{6}
$$

In the above equation, E_{11}^{csm} and E_{22}^{csm} are the moduli based on the following equations, (Chamis, 1984)

$$
\begin{aligned}
E_{11}^{csm} &= E_f \cdot v_{ef}^{csm} + E_m \cdot v_{em}^{csm} \\
E_{22}^{csm} &= \frac{E_m}{1-\sqrt{v_{ef}^{csm}} \cdot (1-\frac{E_m}{E_f})}
\end{aligned}
\tag{7}
$$

Using the elastic moduli from Equation 5, the stiffness components of the roving layer reinforcements, Q_{ij}^{rov}, are calculated by the equations of orthotropic materials as follows:

$$
\begin{aligned}
Q_{11}^{rov} &= \frac{E_{11}^{rov}}{1-\nu_{12}^{rov} \cdot \nu_{21}^{rov}} \\
Q_{22}^{rov} &= \frac{E_{22}^{rov}}{1-\nu_{12}^{rov} \cdot \nu_{21}^{rov}} \\
Q_{12}^{rov} &= \frac{\nu_{12}^{rov} \cdot E_{22}^{rov}}{1-\nu_{12}^{rov} \cdot \nu_{21}^{rov}} = Q_{21}^{rov} \\
Q_{66}^{rov} &= G_{12}^{rov}
\end{aligned}
\tag{8}
$$

The stiffness components of the CSM layer reinforcements, Q_{ij}^{csm}, can be obtained by Equation 9, in which the CSM layer elastic moduli are from Equation 6.

$$Q_{11}^{csm} = Q_{22}^{csm} = \frac{E^{csm}}{1-(\nu^{csm})^2}$$
$$Q_{12}^{csm} = Q_{21}^{csm} = \frac{\nu^{csm} \cdot E^{csm}}{1-(\nu^{csm})^2} \quad (9)$$
$$Q_{66}^{csm} = G^{csm}$$

Table 3 shows the numerical results for the roving layer reinforcements obtained from substituting the material properties in Equations 5 and 8, and Table 4 shows the results for the CSM layer reinforcements from Equations 6 and 9.

Table 3: Lamina Elastic Constants and Stiffnesses of Roving Layer

E_{11} GPa (Msi)	E_{22} GPa (Msi)	G_{12} GPa (ksi)	v
28.1 (4.08)	9.0 (1.31)	3.3 (484)	0.31
Q_{11} GPa (Msi)	Q_{22} GPa (Msi)	Q_{12} GPa (ksi)	Q_{66} GPa (ksi)
29.0 (4.20)	9.3 (1.35)	2.8 (413)	3.3 (484)

Table 4: Lamina Elastic Constants and Stiffnesses of CSM Layer

E GPa (Msi)	G GPa (ksi)	v
16.2 (2.35)	5.8 (837)	0.4
Q_{11} GPa (MSi)	Q_{12} GPa (ksi)	Q_{66} GPa (ksi)
19.3 (2.80)	7.8 (1,126)	5.8 (837)

2.2 Laminate Properties

Considering a laminate consisting of n lamina reinforcement layers, as shown in Figure 2, the extensional stiffnesses, A_{ij}, and the bending stiffnesses, D_{ij}, of the laminate are in the form of Equation 10 and Equation 11, respectively.

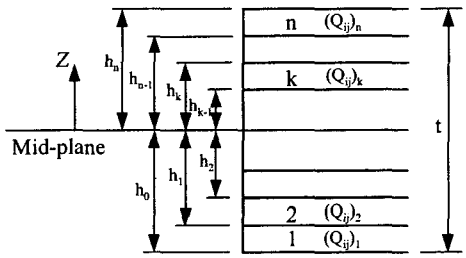

Figure 2: Laminate Geometry and Lamina Stiffnesses

$$A_{ij} = \sum_{k=1}^{n}(Q_{ij})_k \cdot \int_{h_{k-1}}^{h_k} dz = \sum_{k=1}^{n}(Q_{ij})_k \cdot (h_k - h_{k-1}) \quad (10)$$

$$D_{ij} = \sum_{k=1}^{n}(Q_{ij})_k \cdot \int_{h_{k-1}}^{h_k} z^2 dz = \frac{1}{3}\sum_{k=1}^{n}(Q_{ij})_k \cdot (h_k^3 - h_{k-1}^3) \quad (11)$$

Taking the inverse of in-plane and out-of-plane constitutive equations leads to the strain-resultant

force relation and the curvature-resultant moment relation as follows:

$$\begin{Bmatrix} \epsilon_L^0 \\ \epsilon_T^0 \\ \gamma_{LT} \end{Bmatrix} = \frac{1}{A_{11}A_{22} - A_{12}^2} \begin{bmatrix} A_{22} & -A_{12} & 0 \\ -A_{12} & A_{11} & 0 \\ 0 & 0 & \frac{A_{11}A_{22} - A_{22}^2}{A_{66}} \end{bmatrix} \begin{Bmatrix} N_L \\ N_T \\ N_{LT} \end{Bmatrix} \tag{12}$$

$$\begin{Bmatrix} \kappa_L \\ \kappa_T \\ \kappa_{LT} \end{Bmatrix} = \frac{1}{D_{11}D_{22} - D_{12}^2} \begin{bmatrix} D_{22} & -D_{12} & 0 \\ -D_{12} & D_{11} & 0 \\ 0 & 0 & \frac{D_{11}D_{22} - D_{22}^2}{D_{66}} \end{bmatrix} \begin{Bmatrix} M_L \\ M_T \\ M_{LT} \end{Bmatrix} \tag{13}$$

where the resultant forces, N, and the resultant moments, M, are described in Figure 3.

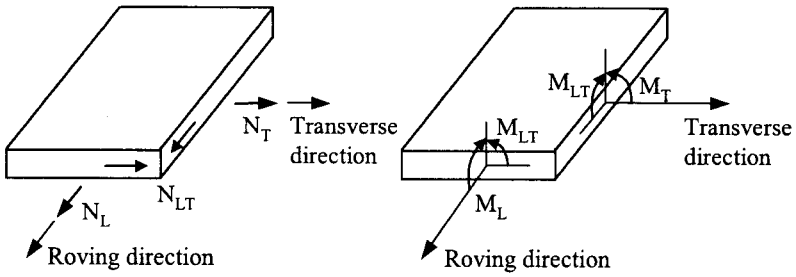

Figure 3: Resultant Forces and Moments

For the case in which the load is applied in the direction of the roving (Figure 3), which also coincides with the material principal direction 1 in Figure 1, Equation 12 is simplified to

$$\epsilon_L^0 = \frac{A_{22}}{A_{11}A_{22} - A_{12}^2} N_L \tag{14}$$

Then the apparent elastic modulus in the roving direction, E_L, is obtained from:

$$E_L = \frac{\sigma_L}{\epsilon_L^0} = \frac{A_{11}A_{22} - A_{12}^2}{A_{22} \cdot t} \tag{15}$$

For the case of the out-of-plane moment M_L, shown in Figure 3, Equation 13 is simplified to

$$\kappa_L = -\frac{\partial^2 w}{\partial x^2} = -\frac{D_{22}}{D_{11}D_{22} - D_{12}^2} M_L \tag{16}$$

Considering w = w (x) and

$$\frac{d^2w}{dx^2} = -\frac{M_L}{E_L^b I} = -\frac{bM_L}{E_L^b(\frac{bt^3}{12})} \tag{17}$$

The apparent flexural modulus, E_L^b, of the pultruded material becomes

$$E_L^b = \frac{12\,(D_{11}D_{22} - D_{12}^2)}{t^3 D_{22}} \tag{18}$$

Table 5 shows values of the apparent moduli E_L and E_L^b predicted by using Equations 15 and 18, respectively. These values compare well with those obtained experimentally.

Table 5: Predicted and Experimental Elastic Moduli of E_L and E_L^b

	E_L GPa (ksi)	E_L^b GPa (ksi)
Predicted	23.97 (3,476)	22.32 (3,237)
Experiment	23.75 (3,445)	21.80 (3,161)
Experiment/Predicted	0.99	0.98

2.3 Sensitivity Analysis

The sensitivities of the moduli E_L (Equation 15) and E_L^b (Equation 18) were evaluated with respect to the variations of major input variables in the predictive models. Table 6 shows the sensitivity evaluation results of the moduli pertaining to the 10% increase of main input variables. As expected, it was observed that the fiber modulus, E_f, showed the highest sensitivity in increasing the moduli, E_L and E_L^b, while the resin volume fraction, v_{re}, showed the highest sensitivity in decreasing the moduli.

Table 6: Moduli Change per 10% Increase of Input Variable

	E_L		E_L^b	
	ΔE_L GPa (ksi)	$\Delta E_L/E_L$%	ΔE_L^b GPa (ksi)	$\Delta E_L^b/E_L^b$ %
E_f	2.01 (291.9)	8.4	1.79 (260.2)	8.0
E_{re}	0.36 (52.8)	1.5	0.41 (59.9)	1.9
E_{fil}	0.01 (1.2)	0.03	0.01 (1.21)	0.04
v_{rov}	0.82 (118.7)	3.4	0.75 (109.1)	3.4
v_{csm}	0.44 (64.4)	1.9	0.41 (59.0)	1.8
v_{re}	-1.02 (-147.4)	-4.2	-0.94 (-136.7)	-4.2
v_{fil}	-0.01 (-2.0)	-0.06	-0.01 (-1.8)	-0.06
v_v	-0.002 (-0.3)	-0.009	-0.002 (-0.3)	-0.009

2.4 Probabilistic Assessment

The characteristics of the analytical predictions of E_L and E_L^b were simulated based on the inherent uncertain properties of the primitive variables by using a probabilistic approach (Liaw et al., 1993, and Shiao et al., 1993) shown schematically in Figure 4. The primitive variables used in the simulations were the constituent elastic properties and the constituent volume fractions whose probabilistic properties are shown in Table 7. The COV's of the moduli and Poisson's ratios of constituents were assumed to be 5% as discussed by Shiao et al. (1993), and the other COV's were from sample tests.

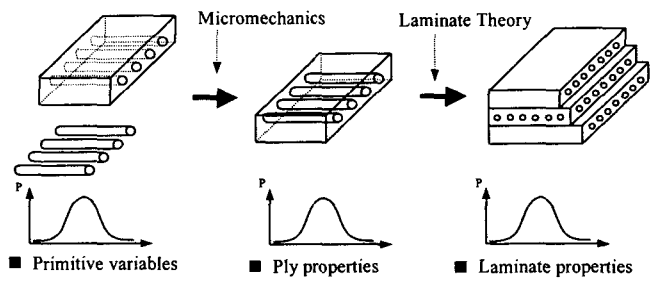

Figure 4: Probabilistic Assessment of Laminate Material Properties

Table 7: Primitive Variable Properties

	Unit	Distribution	Mean	STD	COV
E_f	GPa (ksi)	Normal	72 (10,500)	3.60 (525)	5.0%
v_f	-	Normal	0.2	0.01	5.0%
E_{re}	GPa (ksi)	Normal	3.4 (490)	0.17 (25)	5.0%
v_{re}	-	Normal	0.366	0.018	5.0%
E_{fil}	GPa (ksi)	Normal	20.0 (2,900)	1.0 (145)	5.0%
v_{fil}	-	Normal	0.3	0.015	5.0%
υ_{rov}	%	Normal	23.1	1.43	6.2%
υ_{csm}	%	Normal	12.2	0.82	6.7%
υ_{re}	%	Normal	53.7	1.24	2.3%
υ_{fil}	%	Normal	9.3	1.12	12.0%
υ_v	%	Normal	1.7	0.22	12.9%

Table 8 shows the probabilistic assessment results of the moduli E_L and E_L^b, which were simulated by using the Monte Carlo method based on the probabilistic properties of the primitive variables in Table 7. The experimental values of the moduli are also presented in Table 8. Each simulated datum in Table 8 represents 1,000 observations generated by the Monte Carlo method.

Table 8: Probabilistic Assessment and Experimental Vlaues of E_L and E_L^b

	E_L GPa (ksi)		E_L^b GPa (ksi)	
	Probabilistic Assessment	Experiment	Probabilistic Assessment	Experiment
Mean	23.99 (3,480)	23.75 (3,445)	22.35 (3,241)	21.80 (3,161)
STD	1.21 (175)	1.50 (218)	1.10 (159)	2.32 (337)
COV	5.0%	6.3%	4.9%	10.7%
$X_{p=0.05}$	22.07 (3,201)	21.29 (3,088)	20.60 (2,988)	17.99 (2,609)

3. CONCLUSION

In this study, the elastic properties of pultruded FRP composite components (E_L and E_L^b) have been estimated based on micromechanics models and classical laminate theory (CLT), and probabilistic assessments have been carried out for the prediction models.

1. The micromechanics models for the pultruded composite moduli, E_L and E_L^b, show good prediction results compared with experimental data.

2. The prediction models have the highest sensitivity to the fiber modulus E_f in increasing the moduli, and the highest sensitivity to the resin volume fraction υ_{re} in decreasing the moduli.

3. Probabilistic assessments for the prediction models show that the models well represent the probabilistic characteristics of the composite moduli based upon the inherent uncertainties of primitive variables, such as constituent material properties, fabrication process variables, and geometry of composites.

BIBLIOGRAPHY

1. Agarwal, B.D. and Broutman, L.J. (1990), *Analysis and Performance of Fiber Composites*, John Wiley & Sons, Inc., New York, NY.
2. Chamis, C.C, (1984), "Simplified Composite Micromechanics Equations for Hygral, Thermal, and Mechanical Properties," SAMPE Quarterly, Vol. 15, No. 3, pp. 14-23.
3. Katz, H.S. and Mileswski, J.V. (1978), *Handbook of Fillers and Reinforcements for Plastics*, Van Nostrand Reinhold Co., New York, NY.
4. Liaw, D.G., Singhal, S.N., Murthy, P.L.N., and Chamis, C.C. (1993), "Quantification of Uncertainties in Composites," Collection of Technical Papers, AIAA/ASME Structures, Structural Dynamics and Materials Conference, pt. 2, AIAA, pp. 1163-1173.
5. Mallick, P.K. (1993), *Fiber-reinforced Composites: Materials, Manufacturing, and Design.*, Marcel Dekker, Inc., New York, NY.
6. Mura, T. (1987), *Micromechanics of Defects in Solids*, 2nd ed., Kluwer Academic Publishers.
7. Shiao, M.C., Abumeri, G.H., and Chamis, C.C. (1993), "Probabilistic Assessment of Composite Structures," Collection of Technical Papers, AIAA/ASME Structures, Structural Dynamics and Materials Conference, pt. 2, AIAA, pp. 1173-1186.
8. Tsai, S.W. and Pagano, N.J. (1968), "Invariant Properties of Composite Materials," Composite Materials Workshop, Technomic Publishing Co., Stamford, Conn. p. 233.